Combining next-to-leading order QCD and electroweak radiative corrections to W-boson production at hadron colliders in the POWHEG framework

C. Bernaciak*

Institut für Theoretische Physik, Universität Heidelberg, D-69120 Heidelberg, Germany

D. Wackeroth†

Department of Physics, SUNY at Buffalo, Buffalo, New York 14260-1500, USA

(Received 3 February 2012; published 7 May 2012)

The precision measurement of the mass of the W boson is an important goal of the Fermilab Tevatron and the CERN Large Hadron Collider (LHC). It requires accurate theoretical calculations which incorporate both higher-order QCD and electroweak corrections, and also provide an interface to parton-shower Monte Carlo programs which make it possible to realistically simulate experimental data. In this paper, we present a combination of the full $\mathcal{O}(\alpha)$ electroweak corrections of WGRAD2, and the next-to-leading order QCD radiative corrections to $W \to \ell\nu$ production in hadronic collisions in a single event generator based on the POWHEG framework, which is able to interface with the parton-shower Monte Carlo programs PYTHIA and HERWIG. Using this new combined QCD + EW Monte Carlo program for W production, we provide numerical results for total cross sections and kinematic distributions of relevance to the W mass measurement at the Tevatron and the LHC for the processes pp, $p\bar{p} \to W^{\pm} \to \mu^{\pm}\nu_{\mu}$. In particular, we discuss the impact of EW corrections in the presence of QCD effects when including detector resolution effects.

DOI: 10.1103/PhysRevD.85.093003 PACS numbers: 14.70.Fm, 12.38.−t, 12.38.Bx, 13.40.Ks

I. INTRODUCTION

The precision measurement of the mass of the W-boson, M_W, is an important goal of the Fermilab Tevatron [1–3] and the CERN Large Hadron Collider (LHC). With precise knowledge of M_W and the top quark mass, m_t, indirect information on the mass of the Higgs boson, M_H, within the standard model (SM) can be extracted from the M_H dependence of radiative corrections to the W mass. Global SM fits to all electroweak precision data performed by the Gfitter Collaboration and the LEP Electroweak Working Group predict the SM Higgs mass to be $M_H = 96^{+31}_{-24}$ GeV (1σ) [4,5] and $M_H = 92^{+34}_{-26}$ GeV (68% C.L.) [6], respectively, which lies well within the mass range presently probed by the Tevatron [7] and LHC [8,9] experiments. Future more precise measurements of the W and top quark masses together with improvements in the SM predictions of M_W are expected to considerably improve the indirect determination of M_H. At the Tevatron, with an integrated luminosity of up to $\mathcal{L} = 4.3$ fb^{-1}, a precision of $\delta M_W = 16$ MeV for the W mass has been reached [3]. For the LHC, estimates range from $\delta M_W = 7$ MeV [11] to $\delta M_W = 20$ MeV [12] for $\mathcal{L} = 10$ fb^{-1}, depending on the assumptions made for detector resolutions and theoretical uncertainties. With a dedicated program [13], one may be able to achieve $\delta M_W = \mathcal{O}(10$ MeV$)$.

In hadronic collisions, the W boson mass can be determined from the transverse mass distribution of the lepton pair, $M_T(l\nu)$, originating from the W decay, $W \to \ell\nu$, and the transverse momentum distribution of the charged lepton or neutrino. Both QCD and electroweak (EW) corrections play an important role in the measurement of W observables at hadron colliders. It is imperative to control predictions for observables relevant to W production at least at the 1% level. Also, the transverse momentum distribution of the W boson is an important ingredient in the current W mass measurement at the Tevatron (see, e.g., Ref. [10] for a review). In lowest order (LO) in perturbation theory, the W boson is produced without any transverse momentum. Only when QCD corrections are taken into account does the W boson acquire a non-negligible transverse momentum, p_T^W. For a detailed understanding of the p_T^W distribution, it is necessary to resum the soft gluon emission terms, and to model nonperturbative QCD corrections. This has been done either by using calculations targeted specifically for resummation and parametrizing nonperturbative effects (see, e.g., Refs. [14,15]), or interfacing a calculation of W boson production at next-to-leading order (NLO) in QCD with a parton-shower Monte Carlo (MC) program and tuning the parameters used to describe the nonperturbative effects. This approach has been pursued in Refs. [16–18], for instance. Fixed higher-order predictions beyond NLO are known for fully differential distributions through next-to-next-to-leading order in QCD [19–21], and recently first steps towards a calculation of the complete mixed EW-QCD $\mathcal{O}(\alpha_s\alpha)$ corrections to the Drell-Yan production process were made in Ref. [22].

While QCD corrections only indirectly affect the W mass extracted from the $M_T(l\nu)$ distribution, EW radiative

*C.Bernaciak@ThPhys.Uni-Heidelberg.de
†dow@ubpheno.physics.buffalo.edu

corrections can considerably distort the shape of this distribution in the region sensitive to the W mass. For instance, final-state photon radiation is known to shift M_W by $\mathcal{O}(100\ \mathrm{MeV})$ [1,2,23–28]. In the last few years, significant progress in our understanding of the EW corrections to W boson production in hadronic collisions has been made. The complete $\mathcal{O}(\alpha)$ EW radiative corrections to $p\overset{(-)}{p} \to W^{\pm} \to \ell^{\pm}\nu$ ($\ell = e, \mu$) were calculated by several groups [29–35] and found to agree [36,37]. First steps towards going beyond fixed-order in QED radiative corrections in W production were taken in Refs. [38–42], for instance, by including the effects of final-state multiple photon radiation. For a review of the state-of-the-art of predictions for W production at hadron colliders see, e.g., Refs. [36,37,43].

As a result of all these studies, given the anticipated accuracy of a W boson mass measurement at the Tevatron and the LHC, it has become increasingly clear, that it is necessary to not only fully understand and control the separate higher-order QCD and EW corrections, but also their combined effects. A first study of combined effects can be found in Ref. [44], where final-state photon radiation was added to a calculation of W boson production which includes NLO and resummed QCD corrections. This study showed that the difference in the effects of EW corrections in the presence of QCD corrections and of simply adding the two predictions may be not negligible in view of the anticipated precision. Moreover, in the relevant kinematic region, i.e., around the Jacobian peak, the QCD corrections tend to compensate some of the effects of the EW corrections. In Ref. [45] the full set of EW $\mathcal{O}(\alpha)$ corrections of HORACE [34] and the QCD NLO corrections to W production were combined in the MC@NLO framework [16] which is interfaced with the parton-shower MC program HERWIG [46]. The results of a combination of the EW $\mathcal{O}(\alpha)$ corrections to W production as implemented in SANC [33] with PYTHIA [47] and HERWIG can be found in Ref. [48], without, however, performing a matching of NLO QCD corrections to the parton shower.

In this paper, we present a combination of the full EW $\mathcal{O}(\alpha)$ radiative corrections of Refs. [30,32] contained in the public MC code WGRAD2 and the QCD corrections to $W \to \ell\nu$ production of POWHEG-W [17]. One advantage of the POWHEG method [49–51] for the use in a detector simulation is that it only generates positive weighted events. Moreover, it provides an interface to both HERWIG and PYTHIA. It is well suited as a starting point for combining EW and QCD corrections to W-boson production in one MC program to serve as an analysis tool in the W-mass measurement of the Tevatron and LHC experiments. The resulting MC code, called in the following POWHEG-W_EW, is publicly available at the POWHEG BOX webpage [52] and allows the simultaneous study of the effects of both QCD and NLO EW corrections with both PYTHIA and HERWIG. We do not include the effects of photon-induced processes and of multiple photon radiation. As has been found in earlier studies [37–42,48], both effects, although small, still can have a non-negligible impact on the W mass measurement and should be included in view of the anticipated final precision of the M_W measurement at the Tevatron. This is left to a future publication.

The technical details of our calculation and implementation of EW $\mathcal{O}(\alpha)$ corrections in POWHEG-W are described in Sec. II. In Sec. III we first describe our cross checks, and then present numerical results for total cross sections and distributions which are of interest for the W-mass measurement at the Tevatron and the LHC. In particular, we study the combined effects of EW $\mathcal{O}(\alpha)$ and QCD corrections on the $M_T(\mu\nu_\mu)$ and $p_T(\mu)$ distributions in $pp, p\bar{p} \to W^{\pm} \to \mu^{\pm}\nu_\mu$, taking into account detector resolution effects and using PYTHIA to simulate parton showering. Finally, our conclusions are presented in Sec. IV.

II. THEORETICAL FRAMEWORK

In the following we concentrate on describing our implementation of the complete EW $\mathcal{O}(\alpha)$ corrections to W production via the Drell-Yan mechanism $q_i\bar{q}_{i'} \to W \to f\bar{f}'(\gamma)$ in POWHEG-W. We refer to the literature for a detailed description of QCD and EW corrections to W boson production at hadron colliders as implemented in POWHEG-W [17] and WGRAD2 [30,32], respectively. To illustrate our implementation, we start with a schematic presentation of the parton-level NLO QCD cross section to W production as given in Ref. [49] (see also Refs. [50,51] for a detailed description of the POWHEG BOX):

$$d\sigma = B(\Phi_2)d\Phi_2 + V(\Phi_2)d\Phi_2 + [R(\Phi_3)d\Phi_3 - C(\Phi_3)d\Phi_3 P], \tag{1}$$

where the $2 \to 3$ phase space of the radiated parton is given by $d\Phi_3 = d\bar{\Phi}_2 d\Phi_{\mathrm{rad}}$, B, V, R denote the Born, virtual and real emission contributions, respectively, and C the counterterms, derived in a suitable subtraction scheme, that ensure that the term in the square brackets is nonsingular. P denotes a projection of $2 \to 3$ kinematics onto $2 \to 2$ kinematics. After some manipulation suitable for interfacing $d\sigma$ with a parton-shower MC, the cross section can be written as follows [49]:

$$d\sigma = \bar{B}(\Phi_2)d\Phi_2\left[\Delta_R^{\mathrm{NLO}}(0) + \Delta_R^{\mathrm{NLO}}(p_T)\frac{R(\Phi_2, \Phi_{\mathrm{rad}})}{B(\Phi_2)}d\Phi_{\mathrm{rad}}\right], \tag{2}$$

where the term in square brackets contains the Sudakov form factor Δ_R^{NLO} and generates the first emission of a light parton, while all subsequent emissions are handled by the parton-shower MC. $\bar{B}$ is defined as [49]

$$\bar{B}(\Phi_2) = B(\Phi_2) + V(\Phi_2) + \int [R(\Phi_2, \Phi_{\rm rad}) - C(\Phi_2, \Phi_{\rm rad})] d\Phi_{\rm rad} \quad (3)$$

and offers a straightforward way of adding the EW corrections to the QCD $\mathcal{O}(\alpha_s)$ corrections contained in V and R. In detail, all changes made to POWHEG-W in order to include the $\mathcal{O}(\alpha)$ EW corrections of WGRAD2 are contained in the $\bar{B}^{f_b}(\Phi_2)$ portion of POWHEG-W and are marked with the subscript "EW" as (now we follow the notation of Ref. [50]):

$$\begin{aligned}\bar{B}^{f_b}(\Phi_2) = {} & [B(\Phi_2) + V_{\rm QCD}(\Phi_2) + V_{\rm EW}(\Phi_2)]_{f_b} + \sum_{\alpha_r=0}^{2} \int \{ d\Phi_{\rm rad} [R_{\rm QCD}(\Phi_3) - C(\Phi_3)] \}_{\alpha_r, f_b}^{\bar{\Phi}_2^{\alpha_r}=\Phi_2} \\ & + \int d\Phi_{\rm rad}^{\alpha_r=0} R_{\rm EW}^{f_b}(\Phi_3) \theta\left(E_\gamma - \delta_s \frac{\sqrt{\hat{s}}}{2}\right) \theta(\hat{s}_{q\gamma} - \delta_c E_\gamma \sqrt{\hat{s}}) \theta(\hat{s}_{\bar{q}\gamma} - \delta_c E_\gamma \sqrt{\hat{s}}) \\ & + \int \frac{dz}{z} \left[\sum_{\alpha_\oplus=1}^{2} G_{{\rm QCD},\oplus}^{\alpha}(\Phi_{2,\oplus}) + G_{{\rm EW},\oplus}^{1}(\Phi_{2,\oplus}) \theta(1 - \delta_s - z) \right]_{f_b} \\ & + \int \frac{dz}{z} \left[\sum_{\alpha_\ominus=1}^{2} G_{{\rm QCD},\ominus}^{\alpha}(\Phi_{2,\ominus}) + G_{{\rm EW},\ominus}^{1}(\Phi_{2,\ominus}) \theta(1 - \delta_s - z) \right]_{f_b}, \end{aligned} \quad (4)$$

where the subscript "QCD" refers to the original POWHEG-W terms. For the real terms, $\alpha_r = 0$ corresponds to singularities occurring when the initial-state emitters are q or $\bar{q}'$ and the gluon could be emitted from either of them. $\alpha_r = 1$ corresponds to a gluon emitting an antiquark, $\bar{q}$ or $\bar{q}'$, and $\alpha_r = 2$ to a gluon emitting a quark q' or q. The f_b correspond to each particular flavor structure at the Born level where in the case of $W \to \ell\nu$ production there are 12.

For each collinear piece, $\alpha_{\oplus(\ominus)} = 1$ corresponds to a quark/antiquark from a hadron with positive (negative) rapidity emitting a collinear gluon and $\alpha_{\oplus(\ominus)} = 2$ to a positive (negative) rapidity gluon emitting a collinear quark/antiquark.

In order to incorporate real photon emission as part of the EW $\mathcal{O}(\alpha)$ corrections, the same momentum used to denote the radiated parton (gluon or quark/antiquark) is used to denote the radiated photon. However, because our implementation of the $\mathcal{O}(\alpha)$ EW corrections does not include photon-induced processes, the EW contribution to the real term of Eq. (4) is incorporated only into the $\alpha_r = 0$ contribution and likewise for the collinear terms there is only an $\alpha_{\oplus,\ominus} = 1$ term, as denoted in Eq. (4).

As described in detail in Ref. [30] (see also Ref. [53]) we use the phase space slicing (PSS) method to extract the soft and collinear singular regions in the contribution of real photon radiation described by $R_{\rm EW}^{f_b}$. In these regions the integration over the photon phase space is performed analytically using a soft and collinear approximation of $R_{\rm EW}^{f_b}$, which is valid as long as the PSS parameters δ_s and δ_c are chosen to be sufficiently small. The soft part is included in $V_{\rm EW}$ and the remnant of the initial-state collinear singularity after mass factorization is denoted by $G_{{\rm EW},(\ominus,\oplus)}^{1}$. Explicit expressions for these contributions and a detailed description of the QED factorization scheme can be found in Ref. [30]. Finally, we refer to the Appendix for the details of this implementation of EW $\mathcal{O}(\alpha)$ corrections into POWHEG-W.

III. NUMERICAL RESULTS

Numerical evaluations of the total cross sections and relevant W boson distributions have been obtained for both Tevatron ($\sqrt{s} = 1.96$ TeV) and LHC ($\sqrt{s} = 7$ TeV) processes using both PYTHIA and HERWIG for QCD parton showering. After a description of the numerical setup in Sec. III A, and of cross checks performed to validate the implementation of the EW corrections of WGRAD2 in POWHEG-W in Sec. III B, we provide results for the total inclusive cross sections with and without parton showering and/or EW corrections in Sec. III C. W boson observables that are relevant to EW precision studies, specifically to the measurement of M_W, are defined and their distributions shown in Sec. III D.

A. Setup

The setup used to obtain the results presented in this paper closely follows Ref. [37]:

(1) *SM input parameters:*
   (i) *Masses:* $M_Z = 91.1876$ GeV, $M_W = 80.398$ GeV, $M_H = 115$ GeV, $m_e = 0.510\,998\,91$ MeV, $m_\mu = 0.1056583668$ GeV, $m_\tau = 1.77684$ GeV, $m_u = 0.06983$ GeV, $m_c = 1.2$ GeV, $m_t = 171.2$ GeV, $m_d = 0.06984$ GeV, $m_s = 0.15$ GeV, $m_b = 4.6$ GeV
   (ii) *W width:* $\Gamma_W = 2.141$ GeV
   (iii) *EW coupling parameters:* $\alpha(0) = 1/137.035999679$, $\cos\theta_w = M_W/M_Z$, $\sin^2\theta_w = 1 - \cos^2\theta_w$
   (iv) *CKM matrix elements:* $|V_{ud}| = |V_{cs}| = 0.975$, $|V_{us}| = |V_{cd}| = 0.222$, $|V_{ub}| = |V_{cb}| = |V_{td}| = |V_{ts}| = 0$, $|V_{tb}| = 1$

(2) *WGRAD2 flags:* qnonr = 0, QED = 4, lfc = 1
(3) *Renormalization/factorization scales:* $\mu_F = \mu_R = \mu = W$ boson invariant mass ($\mu = \mu_{\rm QED} = \mu_{\rm QCD}$)
(4) *Parton distribution function (PDF) sets:* CTEQ10 [54]
(5) *Bare acceptance cuts:* $p_T(l) > 25$ GeV, $p_T(\nu_l) > 25$ GeV, and $|\eta_\ell| < 1$
(6) *Calometric setup:* in addition to bare acceptance cuts, smearing of the four-momenta is applied, and we limit the photon energy for small muon-photon angles as described below.
(7) *Pythia settings:* MSTP(61) = 1, MSTP(71) = 1, MSTJ(41) = 1 which corresponds to all QED showering turned off.

The calometric setup includes smearing of the final-state four-momenta to take into account the uncertainty in the energy measurement in the detector. Gaussian smearing of the final-state four-momenta is simulated with D0 or ATLAS inspired smearing routines. All observables are then calculated from the smeared momenta. Muons are detected in the muon chamber and the requirement that the associated track is consistent with a minimum ionizing particle. Therefore, for muons at the Tevatron and the LHC, we require a small photon energy for small muon-photon opening angles, i.e., we require that $E_\gamma < 2$ GeV for $\Delta R_{\mu\gamma} < 0.1$ and $E_\gamma < 0.1 E_\mu$ for $0.1 < \Delta R_{\mu\gamma} < 0.4$. $\Delta R_{l\gamma}$ denotes the separation of a charged lepton and photon in the pseudorapidity azimuthal angle plane defined as

$$\Delta R_{l\gamma} = \sqrt{\Delta\phi_{l\gamma}^2 + \Delta\eta_{l\gamma}^2}. \tag{5}$$

The results in this paper are obtained in the constant-width scheme and by using the fine structure constant, $\alpha(0)$, in both the LO and NLO EW calculation of the W observables. Since QED radiation has the dominant effect on observables relevant to the W mass measurement, we only include resonant weak corrections (qnonr = 0), i.e., we neglect weak box diagrams. Their impact is important in kinematic distributions away from the resonance region and can be studied by choosing qnonr = 1. We include the full set of QED contributions (QED = 4), i.e., initial-state and final-state radiation as well as interference contributions. The QED and QCD factorization and QCD renormalization scales are chosen to be equal and we assume that the factorization of the photonic initial-state quark mass singularities is done in the QED DIS scheme (lfc = 1). The QED $\overline{\rm MS}$ scheme is implemented as well (lfc = 0) and both schemes are defined in analogy to the corresponding QCD factorization schemes. A description of the QED factorization scheme as implemented in POWHEG-W_EW can be found in Ref. [30].

The fermion masses only contribute to the EW gauge boson self-energies and as regulators of the collinear singularity. The mass of the charged lepton is included in the phase space generation of the final-state four-momenta and serves as a regulator of the singularity arising from collinear photon radiation off the charged lepton. Thus, no collinear cut needs to be applied (collcut = 0 in POWHEG-W_EW) on final-state photon radiation, allowing the study of finite lepton-mass effects. Note that the application of a collinear cut on final-state photon radiation (collcut = 1) is only allowed in the electron case and only when a recombination of the electron and photon momenta is performed in the collinear region (usually defined by $\Delta R_{e\gamma} < R_{\rm cut}$, see Ref. [30] for a detailed discussion). In this paper we present results for the $pp, p\bar{p} \to W^\pm \to \mu^\pm \nu_\mu$ processes in both the bare and calometric setup.

B. Crosschecks

In order to be sure that the EW corrections are properly implemented, a number of crosschecks were performed. In the first, the QCD corrections in POWHEG-W_EW were turned off (i.e., all terms labeled with the subscript "QCD" in Eq. (4) were set to zero) and the numerical results of each piece of the NLO EW corrections (i.e., $V_{\rm EW}$, $G^1_{{\rm EW},(\ominus,\oplus)}$, $R_{\rm EW}$ of Eq. (4)) were compared to WGRAD2. We also compared results for the total inclusive cross section and the $M_T(W)$ and $p_T(\ell)$ distributions obtained with POWHEG-W_EW when only including EW $\mathcal{O}(\alpha)$ corrections with those obtained with WGRAD2. In all these comparisons we found good agreement within the statistical uncertainties of the numerical integration (see also Secs. III C and III D). This is the primary indication that the NLO EW corrections were implemented properly using the numerical phase space integration of the POWHEG BOX. In the second type of crosscheck, the numerical cancellation of the PSS parameters δ_s and δ_c was tested by running POWHEG-W_EW without the NLO QCD corrections (or parton-showering capabilities) of POWHEG-W_EW for different choices of these parameters and observing that the cross sections agree within the statistical error of the numerical integration as long as the PSS parameters are chosen small enough so that the soft/collinear approximation is valid. To illustrate this cancellation we show in Table I the results for the total inclusive cross sections

TABLE I. Results for the total cross sections (in pb) to $pp, p\bar{p} \to W^\pm \to \mu^\pm \nu_\mu$ for different choices of δ_s and δ_c parameters at the Tevatron ($\sqrt{S} = 1.96$ TeV) and LHC ($\sqrt{S} = 7$ TeV). These results reflect the exact (weighted) NLO results of POWHEG-W_EW when only including EW corrections, with bare cuts.

	Tevatron	LHC	
(δ_s,δ_c)	W^+	W^+	W^-
0.01,0.005	362.4(2)	1059.0(5)	758.7(8)
0.01,0.001	362.4(2)	1059.1(7)	759.2(5)
0.001,0.0005	362.3(2)	1059.4(9)	759.4(5)
0.001,0.0001	362.3(2)	1059.2(8)	759.3(5)

for $W^{\pm} \to \mu^{\pm}\nu_{\mu}$ production at the Tevatron and the LHC. Finally, we also checked that the QCD NLO cross sections still coincide with those obtained with the original code, POWHEG-W.

C. Total cross sections

In Tables II and III we present results obtained with POWHEG-W_EW for the total cross sections of $pp, p\bar{p} \to W^{\pm} \to \mu^{\pm}\nu_{\mu}$ processes at the Tevatron with center-of-mass (CM) energy $\sqrt{S} = 1.96$ TeV and the LHC with $\sqrt{S} = 7$ TeV for the bare and calometric setup, respectively. We show results separately for the NLO EW and NLO QCD cross sections and combined NLO EW + QCD results with and without QCD parton shower for both PYTHIA and HERWIG. The NLO EW and QCD results coincide with those that can be obtained with WGRAD2 and POWHEG-W, respectively. At the level of the total cross sections, the combined results can be approximated by simply adding the QCD and EW cross sections. As we will see in Sec. III D, this is not necessarily the case when studying kinematic distributions after applying parton showering. For instance, for W^+ production at the Tevatron (LHC) with bare cuts (see Table II) the EW $\mathcal{O}(\alpha)$ corrections increase the LO total cross section by 3.6%(3.4%), the combined (QCD + EW) corrections increase the QCD cross section at NLO by 3.3% (3.5%) and when parton showering with PYTHIA is included by $3.7 \pm 0.4\%(3.8 \pm 0.4\%)$. When considering the calometric setup (see Table III) the impact of the NLO EW corrections is considerably reduced, and the EW $\mathcal{O}(\alpha)$ corrections increase the LO total cross section by only 1.6%(1.4%), the combined (QCD + EW) corrections increase the QCD cross section at NLO by 1.1%(1.1%) and when parton showering with PYTHIA is included by $1.6 \pm 0.3\%(0.9 \pm 0.3\%)$.

D. Transverse W mass and charged lepton momentum distributions

Differential distributions for the following W-boson observables are shown: transverse mass of the W, $M_T(W)$, and the transverse momentum of the muon, $p_T(\mu)$. The transverse W mass is defined in terms of lepton-neutrino pair observables as

TABLE II. Total cross section results (in pb) of POWHEG-W_EW for $W^{\pm} \to \mu^{\pm}\nu_{\mu}$ production at the Tevatron ($\sqrt{S} = 1.96$ TeV) and the LHC ($\sqrt{S} = 7$ TeV) with bare acceptance criteria as listed in Sec. III A. Shown are results for the LO, NLO EW, NLO QCD, the combined NLO QCD and EW cross sections, as well as results including showering performed with PYTHIA or HERWIG as provided by the POWHEG BOX. The errors shown in parenthesis are statistical errors of the Monte Carlo integration. As a cross check the results of WGRAD2 are provided as well (in square brackets).

	Tevatron		LHC			
	W^+		W^+		W^-	
LO	349.81(2)[349.77(1)]		1024.0(1)[1023.9(1)]		731.69(6)[731.63(2)]	
NLO EW	362.4(2)[362.55(2)]		1059.0(5)[1059.6(1)]		758.7(8)[759.26(3)]	
NLO QCD	384.66(4)		1022.7(2)		750.8(1)	
NLO (QCD + EW)	397.2(2)		1058.0(6)		778(1)	
	PYTHIA	HERWIG	PYTHIA	HERWIG	PYTHIA	HERWIG
LO ⊗ PS	308.4(7)	311.8(7)	854(3)	866(3)	634(2)	639(2)
NLO QCD ⊗ PS	375.3(8)	378.5(8)	1014(3)	1027(3)	744(2)	750(2)
NLO (QCD + EW) ⊗ PS	389.3(8)	393.1(8)	1052(3)	1066(3)	766(2)	774(2)

TABLE III. Total cross section results (in pb) of POWHEG-W_EW for $W^{\pm} \to \mu^{\pm}\nu_{\mu}$ production at the Tevatron ($\sqrt{S} = 1.96$ TeV) and the LHC ($\sqrt{S} = 7$ TeV) with calometric acceptance criteria as listed in Sec. III A. Shown are results for LO, NLO EW, NLO QCD, the combined NLO QCD and EW cross sections, as well as results including showering performed with PYTHIA or HERWIG as provided by the POWHEG BOX. The errors shown in parenthesis are statistical errors of the Monte Carlo integration.

	Tevatron		LHC			
	W^+		W^+		W^-	
LO	320.66(2)		985.62(9)		710.52(6)	
NLO EW	325.9(1)		999.0(5)		715.3(8)	
NLO QCD	369.75(4)		1037.9(2)		758.1(1)	
NLO (QCD + EW)	373.9(1)		1049.0(6)		765(1)	
	PYTHIA	HERWIG	PYTHIA	HERWIG	PYTHIA	HERWIG
LO ⊗ PS	296.3(6)	298.2(6)	853(3)	861(3)	622(2)	626(2)
NLO QCD ⊗ PS	358.4(8)	361.4(8)	1006(3)	1019(3)	736(2)	743(2)
NLO (QCD + EW) ⊗ PS	364.1(8)	366.9(8)	1015(3)	1026(3)	743(2)	751(2)

$$M_T(W) = \sqrt{2p_T(\ell)p_T(\nu)(1-\cos(\Delta\phi_{\ell\nu}))} \qquad (6)$$

with ϕ the azimuthal angle of the charged lepton or neutrino and $\Delta\phi_{\ell\nu}$ the difference between them. Both observables are being used to perform a high-precision W mass measurement at the Tevatron [1,2]. The W mass extracted from these observables is especially sensitive to changes in the line shape in the vicinity of the Jacobian peak. As has been well studied in the literature, final-state photon radiation greatly affects the distributions in this region and predictions for these effects need to be under good theoretical control. Here we will not provide a detailed phenomenological study of these EW effects, which are available in the literature (see, e.g., Ref. [37] for an overview), but rather shall explore how the impact of EW $\mathcal{O}(\alpha)$ corrections is affected by the presence of QCD radiation when considering realistic lepton identification criteria. We only briefly illustrate the main features of the impact of the EW $\mathcal{O}(\alpha)$ corrections on the $M_T(W)$ distribution in Fig. 1 and on the $p_T(l=\mu,e)$ distribution in Fig. 2 when considering the bare and calometric setup by showing the relative corrections defined as

$$\delta_{\rm EW}(\%) = \frac{\frac{d\sigma_{\rm EW}}{d\mathcal{O}} - \frac{d\sigma_{\rm LO}}{d\mathcal{O}}}{\frac{d\sigma_{\rm LO}}{d\mathcal{O}}} \times 100. \qquad (7)$$

The large distortion of the Jacobian peak, especially when only bare cuts are applied, is due to collinear final-state photon radiation which results into large logarithmic enhancements of the form $\alpha\log(m_l^2/\hat{s})$, where m_l denotes the charged lepton mass and $\hat{s}$ the partonic CM energy squared. In the electron case, when realistic experimental conditions are taken into account, the electron and photon four-momentum vectors are recombined to an effective electron four-momentum vector if their separation $\Delta R_{e\gamma}$ in the azimuthal angle—pseudorapidity plane is smaller than a critical value $R_{\rm cut} = 0.1$. In that case, these mass-singular logarithms cancel, and only a small effect of the EW corrections survives. In the muon case, however, the muon is well separated from the photon so that in the calometric setup, the distortion of the $M_T(W)$ and $p_T(\mu)$ distributions around the Jacobian peak is more pronounced than in the electron case. Since the electron case is very sensitive to the details of the lepton identification requirements, a detailed study of combined EW and QCD effects should be performed in collaboration with experimentalists involved in the W mass measurement. We leave such a study to a later publication and concentrate in this paper on discussing the impact of QCD corrections on the EW effects in the muon case. Note that the results presented in Ref. [44] are obtained for the electron case with bare cuts, and therefore larger effects have been observed than it can be the case with a more realistic treatment. Finally, we will only present results for the $W^+ \to \mu^+\nu_\mu$ process, since even at the LHC the EW effects in the $M_T(W)$ and $p_T(\mu)$ distributions are similar in W^+ and W^- production, at least in the kinematic region of interest (note that there is no distinction between W^+ and W^- production at the Tevatron because of the symmetric initial state). Also in the presence of QCD radiation we found that the relative corrections discussed in this paper exhibit very similar features for W^+ and W^- observables at the LHC.

In Figs. 3–6 and 9–12, we provide respectively $M_T(W)$ and $p_T(\mu)$ distributions calculated at LO ⊗ PS, NLO EW,

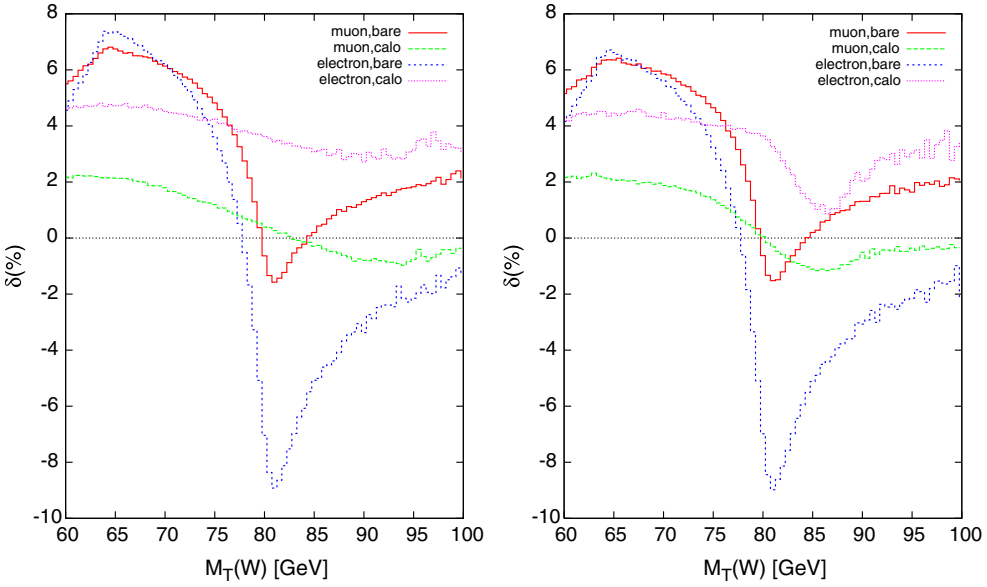

FIG. 1 (color online). Relative corrections $\delta_{\rm EW}$ to the $M_T(W)$ distributions for $p\bar{p} \to W^+ \to e^+\nu_e, \mu^+\nu_\mu$ at $\sqrt{S} = 1.96$ TeV on the left and $pp \to W^+ \to e^+\nu_e, \mu^+\nu_\mu$ at $\sqrt{S} = 7$ TeV on the right obtained with WGRAD2. Bare and calometric cuts are shown for comparison.

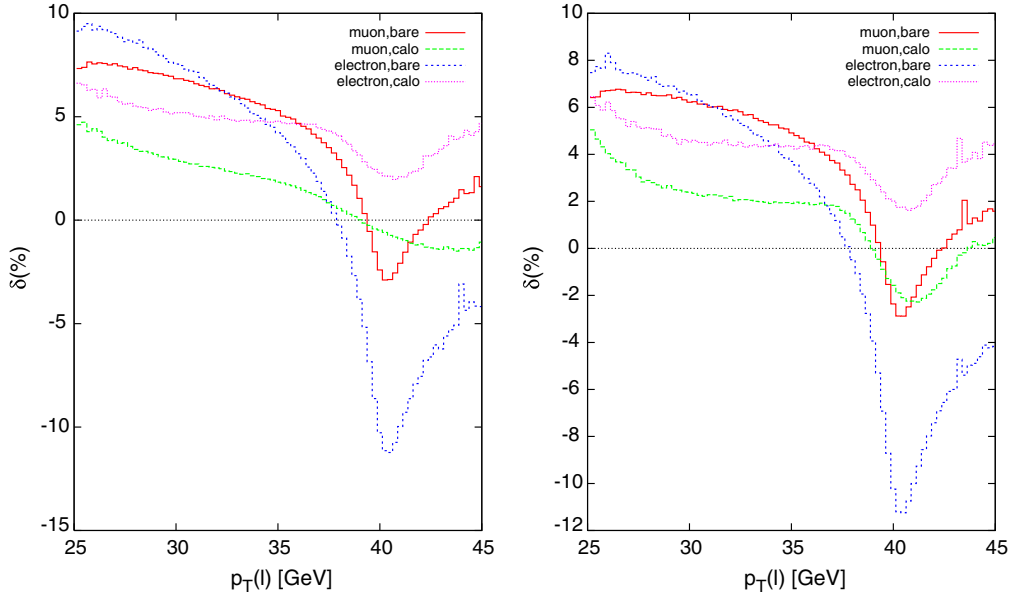

FIG. 2 (color online). Relative corrections δ_{EW} to $p_T(l)$ distributions for $p\bar{p} \to W^+ \to e^+\nu_e, \mu^+\nu_\mu$ at $\sqrt{S} = 1.96$ TeV, on the left and $pp \to W^+ \to e^+\nu_e, \mu^+\nu_\mu$ at $\sqrt{S} = 7$ TeV on the right obtained with WGRAD2. Bare and calometric cuts are shown for comparison.

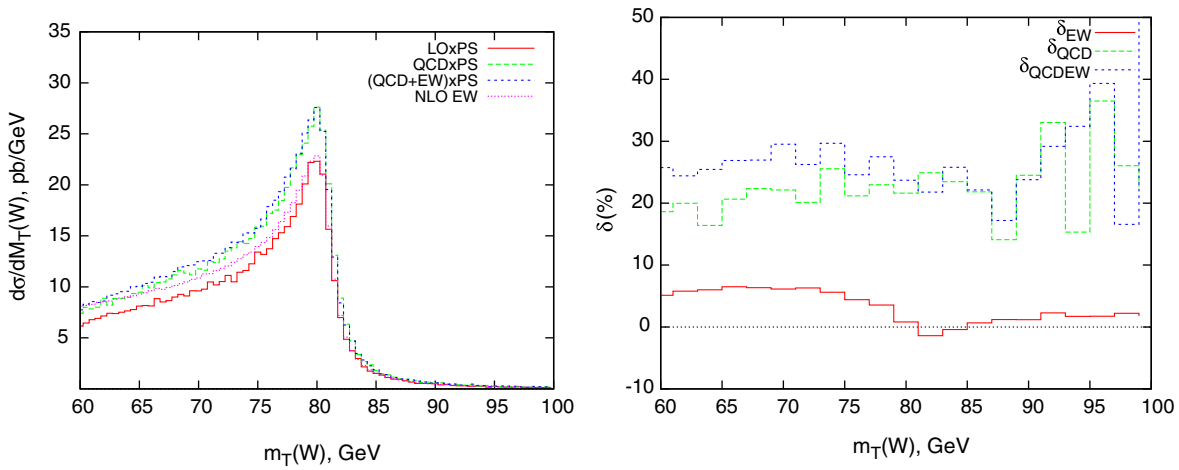

FIG. 3 (color online). $M_T(W)$ distributions and relative corrections δ_{EW}, δ_{QCD}, δ_{QCDEW} for $p\bar{p} \to W^+ \to \mu^+\nu_\mu$, $\sqrt{S} = 1.96$ TeV, obtained with POWHEG-W_EW, with bare cuts. Parton showering (denoted by PS) is performed by interfacing with PYTHIA.

NLO QCD ⊗ PS and NLO (QCD + EW) ⊗ PS as provided by POWHEG-W_EW, where we used PYTHIA to shower the events. We also produced these distributions with HERWIG, but since the effects we are interested in, i.e., the change of the relative impact of EW corrections in the presence of QCD radiation are similar we only show results obtained with PYTHIA. We note that a detailed, tuned comparison of the impact of these two parton-shower MCs on W observables in the presence of the complete EW $\mathcal{O}(\alpha)$ corrections, which is especially important in determining their contribution to the theoretical uncertainty in the extraction of the W mass, can now be conveniently performed with POWHEG-W_EW. To illustrate the impact of the various higher-order corrections on $M_T(W)$ and $p_T(\mu)$ distributions we also show various relative corrections. Apart from δ_{EW} of Eq. (7), we show the impact of QCD corrections (δ_{QCD}) and combined QCD and EW corrections (δ_{QCDEW}) in the presence of a QCD parton shower relative to the LO parton shower result, defined as

$$\delta_{\mathrm{QCD}}(\%) = \frac{\frac{d\sigma_{\mathrm{QCD}\otimes\mathrm{PS}}}{d\mathcal{O}} - \frac{d\sigma_{\mathrm{LO}\otimes\mathrm{PS}}}{d\mathcal{O}}}{\frac{d\sigma_{\mathrm{LO}\otimes\mathrm{PS}}}{d\mathcal{O}}} \times 100, \tag{8}$$

and

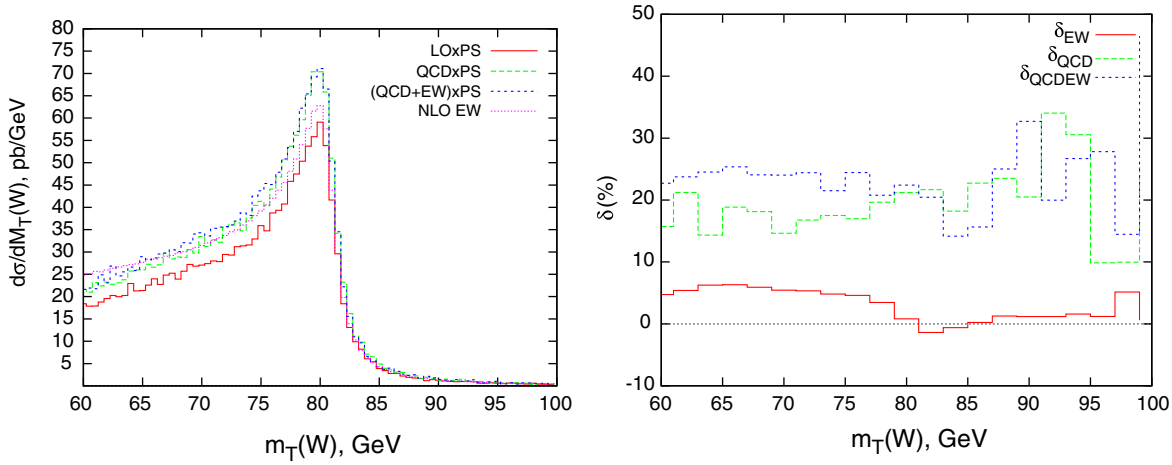

FIG. 4 (color online). $M_T(W)$ distributions and relative corrections δ_{EW}, δ_{QCD}, $\delta_{\mathrm{QCD\,EW}}$ for $pp \to W^+ \to \mu^+ \nu_\mu$, $\sqrt{S} = 7$ TeV, obtained with POWHEG-W_EW, with bare cuts. Parton showering (denoted by PS) is performed by interfacing with PYTHIA.

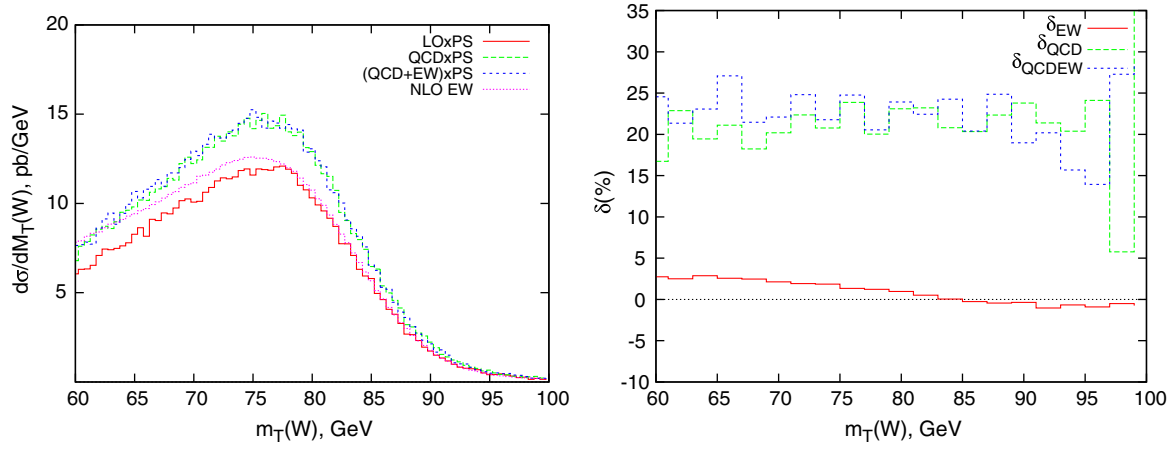

FIG. 5 (color online). $M_T(W)$ distributions and relative corrections δ_{EW}, δ_{QCD}, δ_{QCDEW} for $p\bar{p} \to W^+ \to \mu^+ \nu_\mu$, $\sqrt{S} = 1.96$ TeV, obtained with POWHEG-W_EW, with calometric cuts. Parton showering (denoted by PS) is performed by interfacing with PYTHIA.

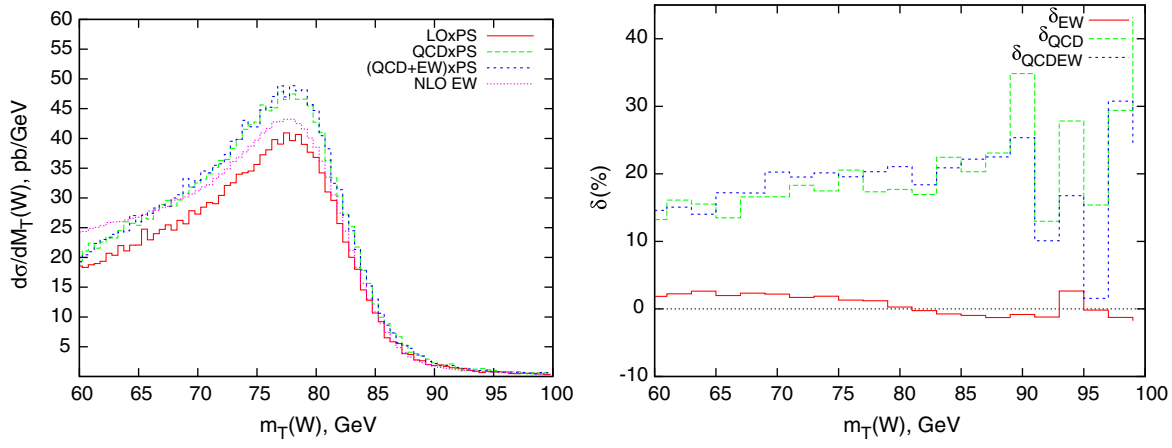

FIG. 6 (color online). $M_T(W)$ distributions and relative corrections δ_{EW}, δ_{QCD}, δ_{QCDEW} for $pp \to W^+ \to \mu^+ \nu_\mu$, $\sqrt{S} = 7$ TeV, obtained with POWHEG-W_EW, with calometric cuts. Parton showering (denoted by PS) is performed by interfacing with PYTHIA.

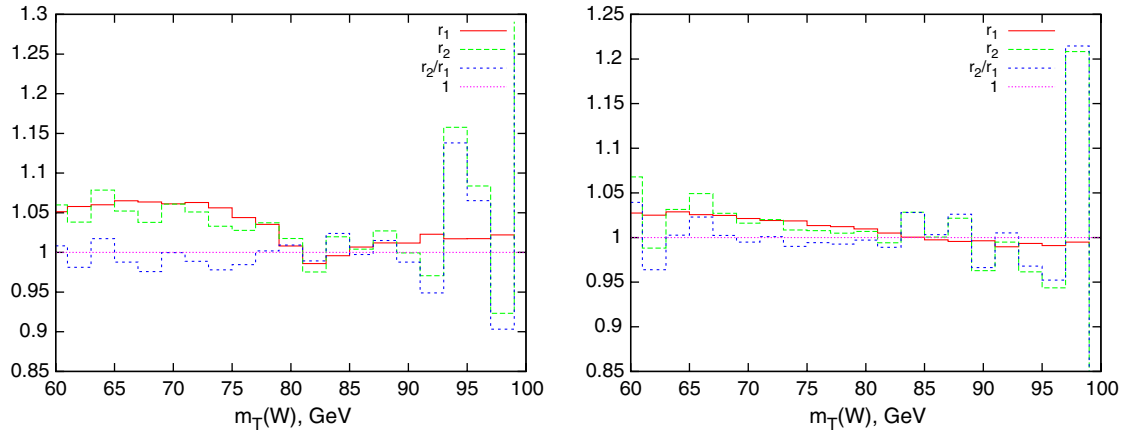

FIG. 7 (color online). Ratios $r_{1,2}$ and their ratio $\mathcal{R}$ for $p\bar{p} \to W^+ \to \mu^+\nu_\mu$, $\sqrt{S} = 1.96$ TeV, obtained with POWHEG-W_EW, with bare (left) and calometric (right) cuts. Parton showering is performed by interfacing with PYTHIA.

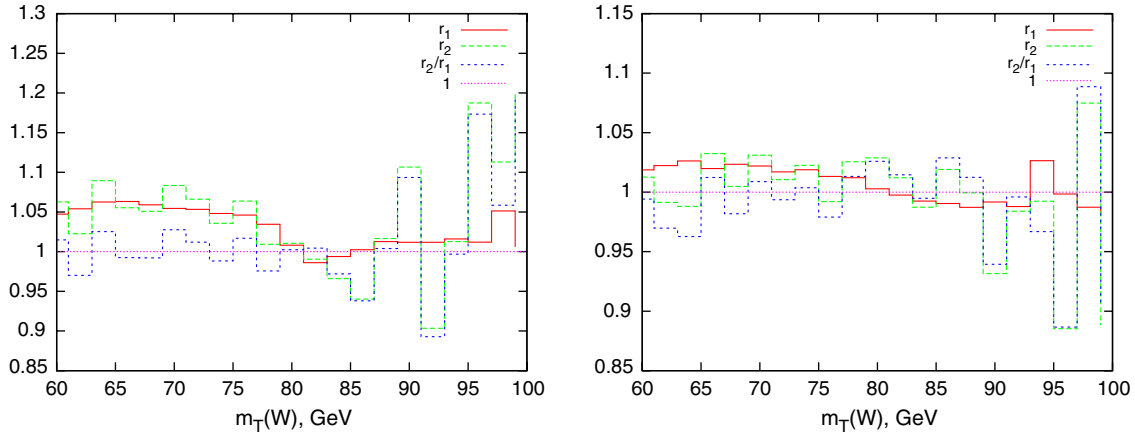

FIG. 8 (color online). Ratios $r_{1,2}$ and their ratio $\mathcal{R}$ for $pp \to W^+ \to \mu^+\nu_\mu$, $\sqrt{S} = 7$ TeV, obtained with POWHEG-W_EW, with bare (left) and calometric (right) cuts. Parton showering is performed by interfacing with PYTHIA.

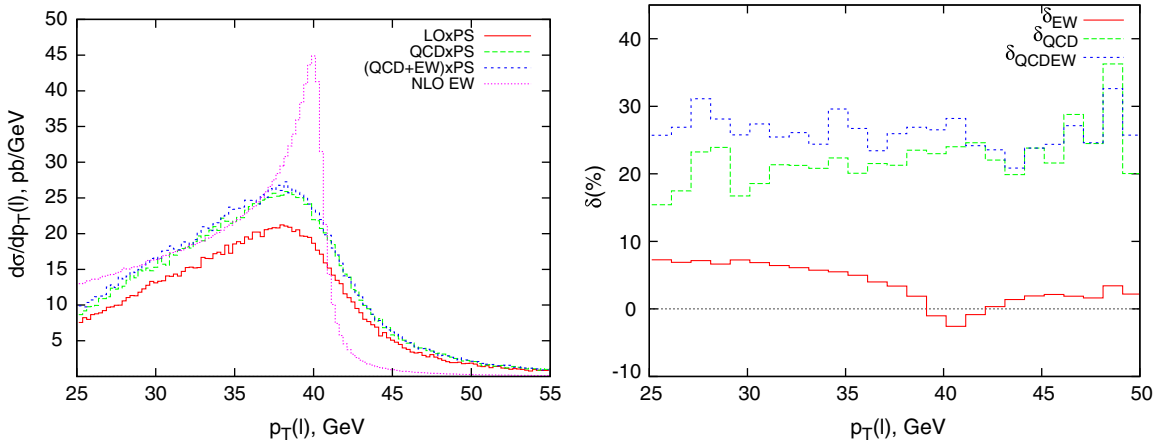

FIG. 9 (color online). $P_T(\mu)$ distributions and relative corrections $\delta_{\rm EW}$, $\delta_{\rm QCD}$, $\delta_{\rm QCD\,EW}$ for $p\bar{p} \to W^+ \to \mu^+\nu_\mu$, $\sqrt{S} = 1.96$ TeV, obtained with POWHEG-W_EW, with bare cuts. Parton showering (denoted by PS) is performed by interfacing with PYTHIA.

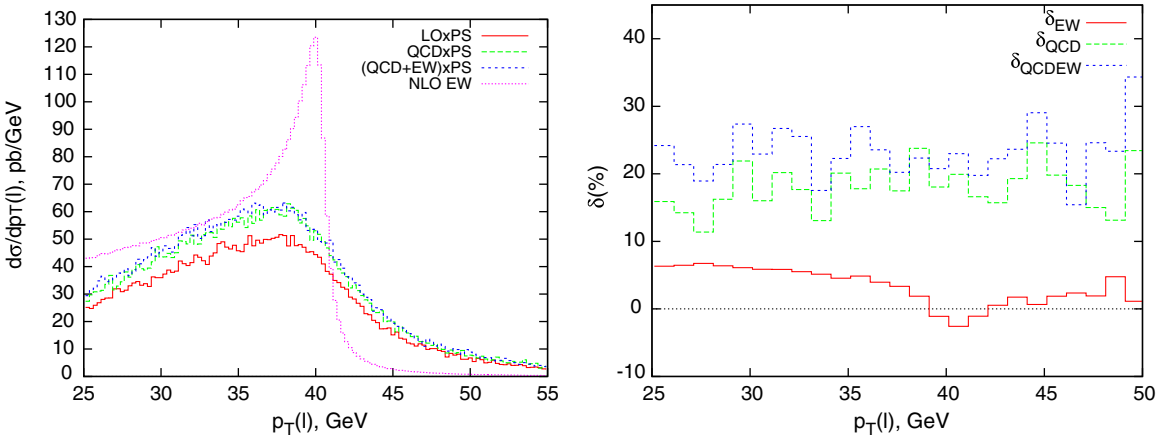

FIG. 10 (color online). $P_T(\mu)$ distributions and relative corrections $\delta_{\rm EW}$, $\delta_{\rm QCD}$, $\delta_{\rm QCD\,EW}$ for $pp \to W^+ \to \mu^+\nu_\mu$, $\sqrt{S} = 7$ TeV, obtained with POWHEG-W_EW, with bare cuts. Parton showering (denoted by PS) is performed by interfacing with PYTHIA.

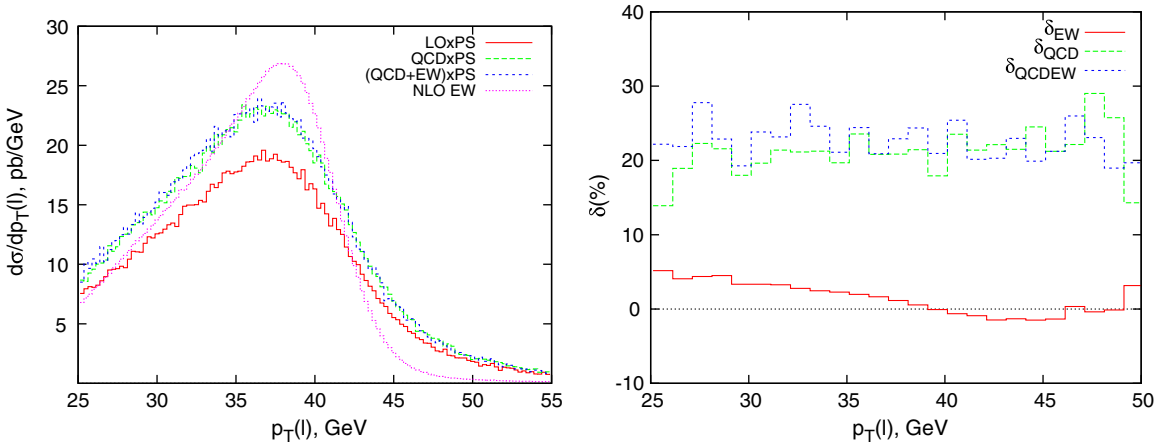

FIG. 11 (color online). $P_T(\mu)$ distributions and relative corrections $\delta_{\rm EW}$, $\delta_{\rm QCD}$, $\delta_{\rm QCDEW}$ for $p\bar{p} \to W^+ \to \mu^+\nu_\mu$, $\sqrt{S} = 1.96$ TeV, obtained with POWHEG-W_EW, with calometric cuts. Parton showering (denoted by PS) is performed by interfacing with PYTHIA.

$$\delta_{\rm QCDEW}(\%) = \frac{\frac{d\sigma_{\rm (QCD+EW)\otimes PS}}{d\mathcal{O}} - \frac{d\sigma_{\rm LO\otimes PS}}{d\mathcal{O}}}{\frac{d\sigma_{\rm LO\otimes PS}}{d\mathcal{O}}} \times 100. \qquad (9)$$

Note that the EW NLO results shown in Figs. 3–6 and 9–12, can be directly compared to and should agree with the results obtained with WGRAD2 shown in Figs. 1 and 2.

Overall, we observe that the impact on the $M_T(W)$ distribution of the EW corrections, $\delta_{\rm EW}$, alone is seen to be slightly negative in the peak region, while the effect of the QCD (NLO and PS), $\delta_{\rm QCD}$, corrections alone consistently increases the LO $\otimes$ PS $M_T(W)$ distribution, as expected. Now, the combined relative NLO (QCD + EW) $\otimes$ PS corrections, $\delta_{\rm QCDEW}$, still follow in magnitude the effect one expects when simply adding NLO QCD $\otimes$ PS and NLO EW corrections, but seems to be slightly different in shape in the peak region at the LHC when applying bare cuts. The dip observed in the relative $\delta_{\rm EW}$ correction seems now to be somewhat washed out.

To study this possible effect of combining EW and QCD corrections more closely, we follow the discussion of Ref. [44], and for each of the observables, we define

$$r_1 = \frac{\frac{d\sigma_{\rm NLO\ EW}}{d\mathcal{O}}}{\frac{d\sigma_{\rm LO}}{d\mathcal{O}}} \qquad r_2 = \frac{\frac{d\sigma_{\rm (QCD+EW)\otimes PS}}{d\mathcal{O}}}{\frac{d\sigma_{\rm QCD\otimes PS}}{d\mathcal{O}}} \qquad (10)$$

and show in Figs. 7 and 8 $r_{1,2}$ together with their ratio $\mathcal{R} = r_2/r_1$. We see that within the statistical uncertainty of the numerical integration, $\mathcal{R}$ is largely consistent with unity, i.e., generally the NLO EW corrections in the presence of QCD effects behave like those of EW alone, only at the LHC there seems to be a slight change in shape above the peak region, but given the large fluctuation in this region this is more likely a relic of the numerical integration. Since QCD radiation is known not to have a significant effect on the shape of the $M_T(W)$ distribution, it is no surprise that the main features of the EW corrections in the presence of QCD corrections are largely unchanged. This has also been observed in Refs. [44,45]. Our results

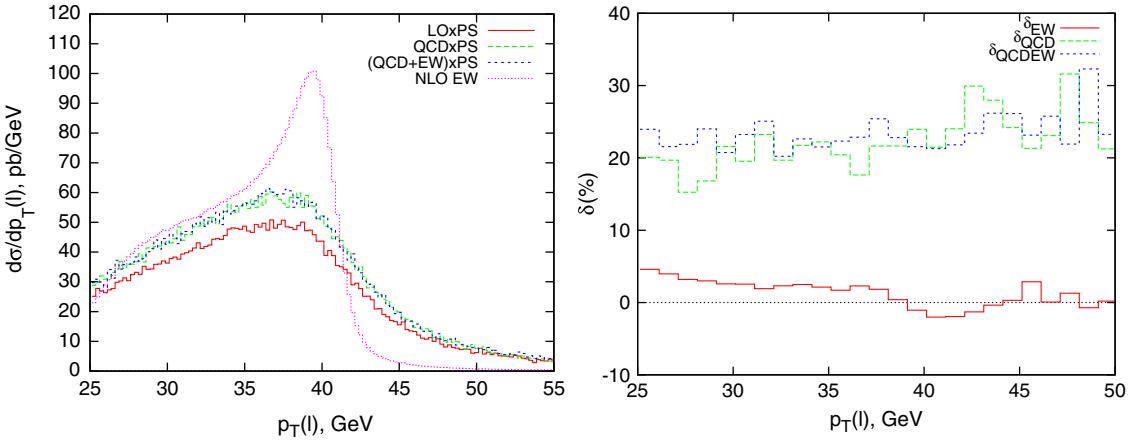

FIG. 12 (color online). $P_T(\mu)$ distributions and relative corrections $\delta_{\rm EW}$, $\delta_{\rm QCD}$, $\delta_{\rm QCDEW}$ for $pp \to W^+ \to \mu^+\nu_\mu$, $\sqrt{S} = 7$ TeV, obtained with POWHEG-W_EW, with calometric cuts. Parton showering (denoted by PS) is performed by interfacing with PYTHIA.

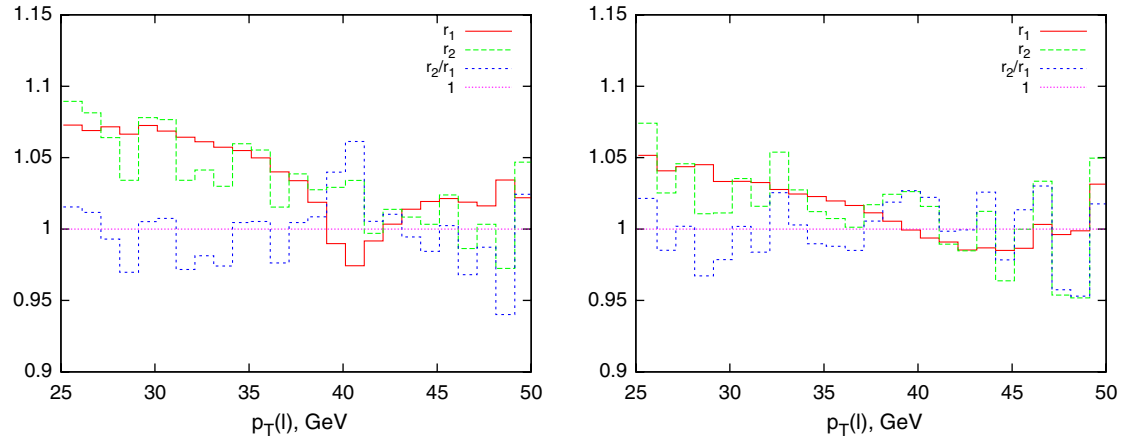

FIG. 13 (color online). Ratios $r_{1,2}$ and their ratio $\mathcal{R}$ for $p\bar{p} \to W^+ \to \mu^+\nu_\mu$, $\sqrt{S} = 1.96$ TeV, obtained with POWHEG-W_EW, with bare (left) and calometric (right) cuts. Parton showering is performed by interfacing with PYTHIA.

cannot be directly compared with earlier studies such as those presented in Refs. [44,45], since in Ref. [44] results are provided for the electron case with bare cuts and in Ref. [45] slightly different selection criteria have been used and the G_μ EW input scheme has been adopted.[1] Nevertheless, the overall features of the effects of combining QCD and EW corrections turn out to be similar. It will be interesting to perform a tuned comparison of different implementations of EW/QED corrections in NLO QCD + resummed calculations of W boson observables, i.e., of POWHEG-W_EW, MC@NLO/HORACE [45] and RESBOS-A [44], which is left to a future publication.

We now turn to the discussion of the $p_T(\mu)$ distributions, and show in the right-hand plots in Figs. 9–12 again the relative corrections $\delta_{\rm EW}$ of Eq. (7), $\delta_{\rm QCD}$ of Eq. (8) and $\delta_{\rm QCDEW}$ of Eq. (9). In contrast to the $M_T(W)$ distribution, now the effects of QCD radiation on the shape of the $p_T(\mu)$ distributions are quite pronounced, as can be seen by comparing the exact NLO EW distribution with the distributions obtained with showered events shown on the left-hand side of Figs. 9–12. So, we expect to see a change in how the EW corrections impact the $p_T(\mu)$ distributions due to a nontrivial interplay of QCD and EW corrections in the combined result. After all, as can be seen in Eq. (2) with $\bar{B}$ of Eq. (4), higher-order QCD-EW interference terms are present and may have a non-negligible impact on the $p_T(\mu)$ distributions. Therefore, it is interesting to note the overall significant shape change between the exact NLO EW and the combined NLO (QCD + EW) ⊗ PS $p_T(\mu)$ distributions. That the NLO EW corrections, in the presence of QCD effects, tend to be quite subdued is obvious in the magnitude and shape of the relative NLO (QCD + EW) ⊗ PS corrections compared to the NLO EW relative corrections, as shown on the right-hand side of these figures. Especially the dip in the Jacobian region

[1]The results obtained in the G_μ scheme can be estimated from our results in the $\alpha(0)$ scheme by $\sigma^{\rm NLO}_{G_\mu} = (\sigma^{\rm NLO}_{\alpha} - 2\Delta r \sigma^{\rm LO}_{\alpha})\alpha^2_{G_\mu}/\alpha(0)^2$ with $\Delta r = 0.0315$, $\alpha_{G_\mu} = \sqrt{2}G_\mu \sin^2\theta^{\rm eff}_w M^2_W/\pi$, and $G_\mu = 1.166\,39 \cdot 10^{-5}$ GeV^{-2}.

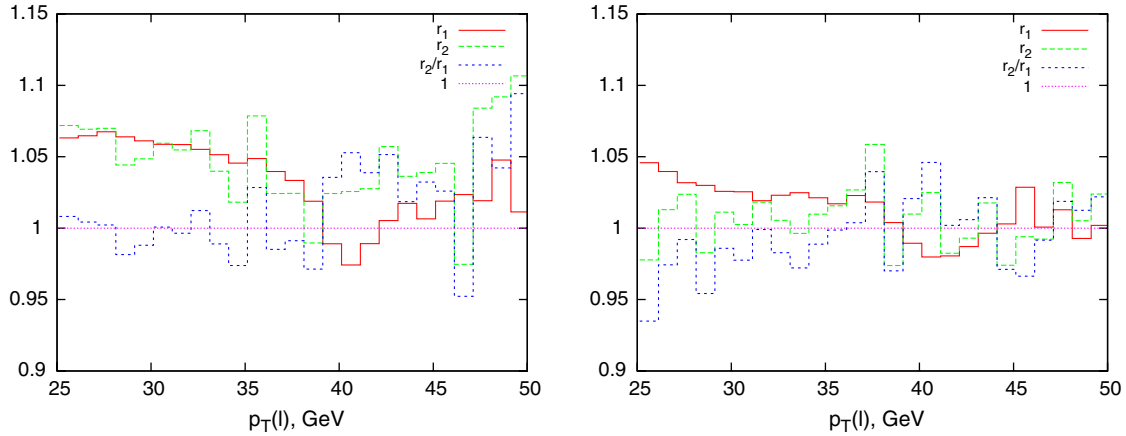

FIG. 14 (color online). Ratios $r_{1,2}$ and their ratio $\mathcal{R}$ for $pp \to W^+ \to \mu^+ \nu_\mu$, $\sqrt{S} = 7$ TeV, obtained with POWHEG-W_EW, with bare (left) and calometric (right) cuts. Parton showering is performed by interfacing with PYTHIA.

from the NLO EW corrections with bare cuts is now mostly washed out.

Again, we study these effects more closely in Figs. 13 and 14 by comparing the impact of NLO EW corrections alone and their impact in the presence of QCD corrections as described by r_1 and r_2 of Eq. (10), respectively. Clearly, unlike in the case of the $M_T(W)$ distribution, r_1 and r_2 are now quite different so that their ratio $\mathcal{R}$ exhibits an interesting shape especially around the Jacobian peak. As expected, in the calometric setup, this difference is much less pronounced due to the smaller impact of the EW corrections on the shape of the $p_T(\mu)$ distributions.

IV. CONCLUSIONS

In this paper we describe the combination of the complete EW $\mathcal{O}(\alpha)$ corrections with NLO QCD + resummed corrections to W production in hadronic collisions, based on implementing the EW corrections of WGRAD2 in POWHEG-W. Using the resulting MC program, POWHEG-W_EW, which is publicly available on the webpage of the POWHEG BOX, we presented results for the transverse W mass and charged lepton momentum distributions, taking into account lepton identification requirements which are closely modeled after those used in the high-precision measurement of the W mass at the Tevatron. In view of the anticipated precision of the W mass measurement at the Tevatron and the LHC, predictions for these observables including higher-order radiative corrections have to be under excellent control. Tools such as POWHEG-W_EW that allow the study of combined EW and QCD corrections are important in reducing the theoretical uncertainty in the W mass measurement. We especially concentrated on studying whether there is a change of the impact of EW corrections when QCD radiation is present as described by POWHEG+PYTHIA in the kinematic region where EW corrections are known to have a significant impact on the extracted W mass. We found interesting QCD-EW interference effects in the $p_T(\mu)$ distributions, i.e., effects that go beyond simply adding QCD and NLO EW corrections, that change the shape of the distribution around the Jacobian peak. These effects are similar to those observed in Refs [44,45], and their impact on the W mass extracted from the $p_T(\mu)$ distribution should be studied in more detail by using realistic detector resolution effects, ideally in close collaboration with the experimentalists performing the W mass measurement. Moreover, these findings also suggest that a calculation of the complete mixed EW-QCD $\mathcal{O}(\alpha\alpha_s)$ corrections is desirable to further reduce the theoretical uncertainty and to obtain an accurate estimate of the theory uncertainty due to missing higher-order corrections. Further improvements that are planned for POWHEG-W_EW include the implementation of the known higher-order QED and EW effects, i.e., beyond NLO, of photon-induced processes, and the usage of an updated PDF that fully considers QED corrections, once available. Since POWHEG-W_EW interfaces to both PYTHIA and HERWIG it is also a convenient tool to perform a tuned comparison of QCD + EW effects when using either parton-shower MC. Finally, since POWHEG-W_EW includes the complete NLO EW corrections, it is interesting to note that the effects of EW Sudakov logarithms that become numerically important in distributions at high energies can now also be studied in the presence of QCD radiation. This is especially interesting for the search for W' bosons at the LHC.

ACKNOWLEDGMENTS

We would like to thank C. Oleari and P. Nason for helpful discussions and their support in making this addition to the POWHEG BOX public. We are grateful to U. Baur, who sadly passed away in November 2010, for his invaluable feedback and support in the beginning stages of this project. This research was supported in part by the National Science Foundation under Grant Nos. NSF-PHY-0547564, NSF-PHY-0757691, and PHY-0705682

and Verbundprojekt: "QCD-Jets in Higgs-Physik und Suchen nach neuer Physik" (05H09VHE). Part of this work was performed at the Institute for Theoretical Particle Physics at the Karlsruhe Institute of Technology (KIT), during D. W.'s visit as a Mercator Fellow, funded by the Deutsche Forschungsgemeinschaft (DFG). D. W. is especially grateful to J. Kühn for his kind hospitality during her stay at the KIT.

APPENDIX

In the following we describe in detail the implementation of each EW piece in Eq. (4), which are added to the QCD contribution after testing if the user requests to include EW corrections (`wgrad2 = 1`). An attempt is made to describe both the analytical pieces in the code as well as their variable names. This is important so the user can be aware of how certain flags affect their values as well as of which part of the EW corrections is contained in each piece. For more explicit expressions of the EW $\mathcal{O}(\alpha)$ corrections see Refs. [29,30,32].

A. THE VIRTUAL+SOFT FINITE PIECE, $V_{\mathrm{EW}}^{f_b}(\Phi_2)$

The quantity $V_{EW}^{f_b}(\Phi_2)$ is defined in POWHEG-BOX/W_EW-BW/VIRTUAL_EW.F. There are two flags which affect the outcome, both can be set in the proper POWHEG input file. Except for `qnonr`, all of the flags are used in the definitions of the other EW terms in Eq. (4). For completeness, the flags and their descriptions are listed below.

(1) `QED`: This flag toggles between different subsets of NLO QED contributions.
   (i) `QED = 1` initial state (IS) photon radiation.
   (ii) `QED = 2` final state (FS) photon radiation.
   (iii) `QED = 3` interference between IS and FS photon radiation.
   (iv) `QED = 4` IS, FS and interference.

Note that the gauge invariant separation into IS and FS QED contributions has been performed according to Ref. [29].

(2) `qnonr`: This flag toggles between the treatment of EW corrections to resonant/nonresonant W production. In the case of resonant W production (`qnonr = 0`), a gauge invariant separation into weak and QED $\mathcal{O}(\alpha)$ corrections and into IS and FS contributions is available according to Ref. [29]. In this case, no weak box diagrams are included and the weak form factors are evaluated at $\hat{s} = M_W^2$.
   (i) `qnonr = 0` excludes the weak box diagrams, corresponds to resonant W production only.
   (ii) `qnonr = 1` includes the weak box diagrams, i.e., includes the complete EW $\mathcal{O}(\alpha)$ corrections to W production.

In choosing `qnonr = 1`, the full set of virtual diagrams are used, including the weak box diagrams which are necessary to describe nonresonant W production. Since in case of nonresonant W production the gauge invariant separation into IS and FS QED contributions according to Ref. [29] is no longer possible, the entire set of real radiation diagrams must be included. Therefore, if choosing `qnonr = 1` the user must also set `QED = 4`.

The contents of $V_{\mathrm{EW}}^{f_b}(\Phi_2)$, without the PDF factors, are now explicitly shown.

$$V_{\mathrm{EW}}^{f_b}(\Phi_2) \sim \mathrm{soft\,(1{:}12)} + \mathrm{virt\,(1{:}12)}. \tag{11}$$

The choice of `qnonr` affects virt(1:12) as follows: For `qnonr = 0`

$$\mathrm{virt\,(1{:}12)} = \mathrm{brborn(1{:}12)}\mathcal{R}e[\mathrm{fvwp(1)_{IS}} + \mathrm{fvwp(2)_{FS}}]\frac{2\pi}{\alpha_s} \tag{12}$$

brborn(1:12) are POWHEG-W's definition of the Born contribution and are equivalent to $\frac{1}{2\hat{s}}\overline{\sum}|M_B|^2$ for each flavor structure. fvwp(1:2) are the modified weak one-loop contributions for resonant W production and are defined in /POWHEG-BOX/W_EW-BW/LIBWEAK.F. The user has the choice to include separately the IS and FS contributions through the proper choice of the `QED` flag. Shown above is the outcome corresponding to `QED = 4`. For `qnonr = 1`,

$$\begin{aligned}\mathrm{virt(1{:}6)} = {} & |\mathrm{CKM(1{:}6)}|^2\frac{\pi^2\alpha^2}{s_W^4}\frac{1}{|\hat{s} - M_W^2 + i\Gamma_W M_W|^2}\frac{1}{2\hat{s}}\frac{1}{3} \\ & \times \mathrm{a2qqw}(\hat{s}, -2k_{\bar{q}}\cdot k_l, -2k_q\cdot k_l, 16(k_{\bar{q}}\cdot k_{\bar{l}})^2)\end{aligned} \tag{13}$$

$$\begin{aligned}\mathrm{virt(7{:}12)} = {} & |\mathrm{CKM(7{:}12)}|^2\frac{\pi^2\alpha^2}{s_W^4}\frac{1}{|\hat{s} - M_W^2 + i\Gamma_W M_W|^2}\frac{1}{2\hat{s}}\frac{1}{3} \\ & \times \mathrm{a2qqw}(\hat{s}, -2k_q\cdot k_l, -2k_{\bar{q}}\cdot k_l, 16(k_q\cdot k_{\bar{l}})^2).\end{aligned} \tag{14}$$

The function a2qqw(...) corresponds to the full weak one-loop contribution and is also defined in /POWHEG-BOX/W_EW-BW/LIBWEAK.F. The soft contributions of Eq. (11) are given by

$$\begin{aligned}\mathrm{soft(1{:}6)} = {} & |\mathrm{CKM(1{:}6)}|^2\frac{\pi^2\alpha^2}{s_W^4}\frac{1}{2\hat{s}}\frac{16}{3} \\ & \times\frac{(k_{\bar{q}}\cdot k_{\bar{l}})^2}{|\hat{s} - M_W^2 + i\Gamma_W M_W|^2} \\ & \times[\mathrm{k_{fac}(2)_{IS}} + \mathrm{k_{fac}(2)_{FS}} + \mathrm{k_{fac}(2)_{int}}]\end{aligned} \tag{15}$$

$$\text{soft(7:12)} = |\text{CKM(7:12)}|^2 \frac{\pi^2\alpha^2}{s_W^4}\frac{1}{2\hat{s}}\frac{16}{3} \times \frac{(k_q\cdot k_{\bar{l}})^2}{|\hat{s}-M_W^2+i\Gamma_W M_W|^2} \times [\mathrm{k_{fac}(1)_{IS}} + \mathrm{k_{fac}(1)_{FS}} + \mathrm{k_{fac}(1)_{int}}]. \tag{16}$$

The $\mathrm{k_{fac}}$(1:2) terms correspond to the finite soft photon contributions and are defined in /POWHEG-BOX/W_EW-BW/LIBQED.F. Again, the case of `QED` = 4 is shown above, but the user can include any or all of these $\mathrm{k_{fac}}$ terms by adjusting this flag. The $\mathrm{k_{fac}}$, and hence the soft contribution depends on the soft PSS parameter, δ_s, and when `collcut` = 1 is chosen also on δ_c.

B. THE COLLINEAR REMNANTS, $G^{1,f_b}_{\mathrm{EW},\oplus}$, $G^{1,f_b}_{\mathrm{EW},\ominus}$

These are defined in /POWHEG-BOX/W_EW-BW/COLLINEAR_EW.F. There is also the inclusion of a new flag, `lfc`:

(i) `lfc`: This flag controls the choice of the QED factorization scheme.
(ii) `lfc` = 0 $\overline{\mathrm{MS}}$ scheme.
(iii) `lfc` = 1 DIS scheme.

POWHEG only implements the QCD $\overline{\mathrm{MS}}$ scheme. Hence, as this flag only applies to the EW portions, one has the option to choose different schemes for the QED and QCD factorization. We now describe analytically the contents of these contributions.

$$G^{1,1:6}_{\mathrm{EW},\oplus} + G^{1,1:6}_{\mathrm{EW},\ominus} = |\mathrm{CKM(1:6)}|^2 \frac{\pi^2\alpha^2}{s_W^4}\frac{1}{2\hat{s}}\frac{16}{3}(k_{\bar{q}}\cdot k_{\bar{l}})^2 \frac{\mathrm{kn\,jacborn}}{|\hat{s}-M_W^2+i\Gamma_W M_W|^2} \times \left[\underbrace{\frac{1}{9}\bar{q}_1\left(\frac{x_1}{z_1},\mu_R\right)q_2(x_2,\mu_R)\frac{\mathrm{splitz1}}{z_1}(1-x_1)}_{\sim G^1_{\oplus,\mathrm{EW}}} + \underbrace{\frac{4}{9}\bar{q}_1(x_1,\mu_R)q_2\left(\frac{x_2}{z_2},\mu_R\right)\frac{\mathrm{splitz2}}{z_2}(1-x_2)}_{\sim G^1_{\ominus,\mathrm{EW}}}\right] \tag{17}$$

$$G^{1,7:12}_{\mathrm{EW},\oplus} + G^{1,7:12}_{\mathrm{EW},\ominus} = |\mathrm{CKM(7:12)}|^2 \frac{\pi^2\alpha^2}{s_W^4}\frac{1}{2\hat{s}}\frac{16}{3}(k_q\cdot k_{\bar{l}})^2 \frac{\mathrm{kn\,jacborn}}{|\hat{s}-M_W^2+i\Gamma_W M_W|^2} \times \left[\underbrace{\frac{4}{9}q_1\left(\frac{x_1}{z_1},\mu_R\right)\bar{q}_2(x_2,\mu_R)\frac{\mathrm{splitz1}}{z_1}(1-x_1)}_{\sim G^1_{\oplus,\mathrm{EW}}} + \underbrace{\frac{1}{9}q_1(x_1,\mu_R)\bar{q}_2\left(\frac{x_2}{z_2},\mu_R\right)\frac{\mathrm{splitz2}}{z_2}(1-x_2)}_{\sim G^1_{\ominus,\mathrm{EW}}}\right]. \tag{18}$$

splitz1 and splitz2 are functions of z_1 and z_2, respectively. For a generic z they are

$$\mathrm{splitz} = \frac{\alpha}{2\pi}\left[\frac{1+z^2}{1-z}\ln\left(\frac{\hat{s}}{\mu_F^2}\frac{z}{(1-z)^2}\frac{\delta_c}{2}\right) + 1 - z - \mathtt{lfc}*\mathtt{fcollz}\right] \tag{19}$$

with

$$\mathrm{fcollz} = \frac{1+z^2}{1-z}\ln\left(\frac{1-z}{z}\right) - \frac{3}{2(1-z)} + 2z + 3. \tag{20}$$

In Eq. (19) above, one sees explicitly the QED factorization scheme dependence. Note that the soft part of the QED PDF counterterm is included in $\mathrm{k_{fac}}$. Also, the dependence on the PSS parameter δ_c is explicitly shown.

C. THE REAL CONTRIBUTION, $R^{f_b}_{\mathrm{EW}}$

$R^{f_b}_{\mathrm{EW}}$ are defined in /POWHEG-BOX/W_EW-BW/REAL_EW.F. As mentioned earlier, POWHEG-W considers not only $q\bar{q}$, but gq and $g\bar{q}$ induced processes, while the calculation of WGRAD2 only includes $q\bar{q}$ induced processes. This is why in Eq. (4) there is only one $R^{f_b}_{\mathrm{EW}}$ contribution corresponding to $\alpha_r = 0$. Also, because the EW calculation was performed with two-cutoff phase-space-slicing this EW contribution is finite. Therefore, care is taken to only return values of $R^{f_b}_{\mathrm{EW}}$ which pass certain criteria, namely, that they be away from the soft or collinear regions of the photon phase space. One can also consider subsets of the real corrections by adjusting the flag `QED` when `qnonr` = 0. The real EW contributions, up to the PDF factors, are proportional to subsets of the QED radiation matrix element squared as follows:

$$R_{\mathrm{EW}}^{f_b} \sim \sum_{f_b} \overline{\sum_{\mathrm{sp,col}}} |M_{2\to 3}|^2 = \sum_{f_b} \overline{\sum_{\mathrm{sp,col}}} |M_{\mathrm{IS}} + M_{\mathrm{FS}}|^2_{f_b} \tag{21}$$

$$= \sum_{f_b} \overline{\sum_{\mathrm{sp,col}}} \underbrace{\left[\underbrace{|M_{\mathrm{IS}}|^2_{f_b}}_{\mathrm{QED}=1} + \underbrace{|M_{\mathrm{FS}}|^2_{f_b}}_{\mathrm{QED}=2} + \underbrace{2\mathcal{R}e[M_{\mathrm{IS}} M^*_{\mathrm{FS}}]_{f_b}}_{\mathrm{QED}=3} \right]}_{\mathrm{QED}=4}. \tag{22}$$

The integration of $R_{\mathrm{EW}}^{f_b}$ over the photon phase space is finite after applying soft and collinear cuts as shown in Eq. (4). The dependence on the PSS parameters is canceled numerically between the contributions describing soft, collinear and real hard photon radiation as discussed in Sec. III B. The default values set in VIRTUAL_EW.F represent optimal choices and should only be changed with care.

[1] T. Aaltonen *et al.* (CDF Collaboration), Phys. Rev. Lett. **99**, 151801 (2007); Phys. Rev. D **77**, 112001 (2008); arXiv:1203.0275.
[2] V. M. Abazov *et al.* (D0 Collaboration), Phys. Rev. Lett. **103**, 141801 (2009).
[3] TEV-EWWG Group CDF and D0 Collaboration, arXiv:1204.0042.
[4] H. Flacher, M. Goebel, J. Haller, A. Hocker, K. Monig, and J. Stelzer, Eur. Phys. J. C **60**, 543 (2009); D. Ludwig, Proc. Sci. ICHEP2010 (2010) 404.
[5] M. Baak, M. Goebel, J. Haller, A. Hoecker, D. Ludwig, K. Moenig, and M. Schott, arXiv:1107.0975.
[6] J. Alcaraz, arXiv:0911.2604.
[7] TEVNPH (Tevatron New Phenomena and Higgs Working Group), CDF, and DO Collaborations, arXiv:1107.5518.
[8] S. Chatrchyan *et al.* (CMS Collaboration), Phys. Lett. B **699**, 25 (2011).
[9] G. Aad *et al.* (ATLAS Collaboration), Eur. Phys. J. C **71**, 1728 (2011).
[10] A. V. Kotwal and J. Stark, Annu. Rev. Nucl. Part. Sci. **58**, 147 (2008).
[11] N. Besson, M. Boonekamp, E. Klinkby, T. Petersen, and S. Mehlhase (ATLAS Collaboration), Eur. Phys. J. C **57**, 627 (2008).
[12] V. Buge, C. Jung, G. Quast, A. Ghezzi, M. Malberti, and T. Tabarelli de Fatis, J. Phys. G **34**, N193 (2007).
[13] M. W. Krasny, F. Dydak, F. Fayette, W. Placzek, and A. Siodmok, Eur. Phys. J. C **69**, 379 (2010).
[14] C. Balazs and C. P. Yuan, Phys. Rev. D **56**, 5558 (1997); R. K. Ellis and S. Veseli, Nucl. Phys. **B511**, 649 (1998).
[15] F. Landry, R. Brock, G. Ladinsky, and C. P. Yuan, Phys. Rev. D **63**, 013004 (2000).
[16] S. Frixione and B. R. Webber, J. High Energy Phys. 06 (2002) 029; S. Frixione, F. Stoeckli, P. Torrielli, B. R. Webber, and C. D. White, arXiv:1010.0819.
[17] S. Alioli, P. Nason, C. Oleari, and E. Re, J. High Energy Phys. 07 (2008) 060.
[18] K. Hamilton, P. Richardson, and J. Tully, J. High Energy Phys. 10 (2008) 015
[19] C. Anastasiou, L. J. Dixon, K. Melnikov, and F. Petriello, Phys. Rev. D **69**, 094008 (2004).
[20] K. Melnikov and F. Petriello, Phys. Rev. Lett. **96**, 231803 (2006).
[21] S. Catani, L. Cieri, G. Ferrera, D. de Florian, and M. Grazzini, Phys. Rev. Lett. **103**, 082001 (2009).
[22] W. B. Kilgore and C. Sturm, Phys. Rev. D **85**, 033005 (2012).
[23] F. Abe *et al.* (CDF Collaboration), Phys. Rev. Lett. **75**, 11 (1995); Phys. Rev. D **52**, 4784 (1995); T. Affolder *et al.* (CDF Collaboration), Phys. Rev. D **64**, 052001 (2001).
[24] S. Abachi *et al.* (D0 Collaboration), Phys. Rev. Lett. **77**, 3309 (1996); B. Abbott *et al.* (D0 Collaboration), Phys. Rev. D **58**, 012002 (1998); **58**, 092003 (1998); Phys. Rev. Lett. **80**, 3008 (1998); **84**, 222 (2000); Phys. Rev. D **62**, 092006 (2000); V. M. Abazov *et al.* (D0 Collaboration), Phys. Rev. D **66**, 012001 (2002).
[25] W. Ashmanskas *et al.* (TEV-EWWG Collaboration), Phys. Rev. D **70**, 092008 (2004) and references therein.
[26] F. Abe *et al.* (CDF Collaboration), Phys. Rev. Lett. **74**, 341 (1995).
[27] T. Affolder *et al.* (CDF Collaboration), Phys. Rev. Lett. **85**, 3347 (2000).
[28] V. M. Abazov *et al.* (D0 Collaboration), Phys. Rev. D **66**, 032008 (2002).
[29] D. Wackeroth and W. Hollik, Phys. Rev. D **55**, 6788 (1997).
[30] U. Baur, S. Keller, and D. Wackeroth, Phys. Rev. D **59**, 013002 (1998).
[31] S. Dittmaier and M. Krämer, Phys. Rev. D **65**, 073007 (2002).
[32] U. Baur and D. Wackeroth, Phys. Rev. D **70**, 073015 (2004).
[33] A. Arbuzov, D. Bardin, S. Bondarenko, P. Christova, L. Kalinovskaya, G. Nanava, and R. Sadykov, Eur. Phys. J. C **46**, 407 (2006); **50**, 505(E) (2007).
[34] C. M. Carloni Calame, G. Montagna, O. Nicrosini, and A. Vicini, J. High Energy Phys. 12 (2006) 016.

[35] V. A. Zykunov, Phys. At. Nucl. **71**, 732 (2008); Eur. Phys. J. direct C **3**, 1 (2001).
[36] C. Buttar *et al.*, arXiv:hep-ph/0604120.
[37] C. E. Gerber *et al.* TeV4LHC-Top and Electroweak Working Group, arXiv:0705.3251.
[38] C. M. Carloni Calame, G. Montagna, O. Nicrosini, and M. Treccani, Phys. Rev. D **69**, 037301 (2004).
[39] W. Placzek and S. Jadach, Eur. Phys. J. C **29**, 325 (2003).
[40] P. Golonka and Z. Was, Eur. Phys. J. C **45**, 97 (2006).
[41] K. Hamilton and P. Richardson, J. High Energy Phys. 07 (2006) 010.
[42] S. Brensing, S. Dittmaier, M. Krämer, and A. Muck, Phys. Rev. D **77**, 073006 (2008).
[43] E. Laenen and D. Wackeroth, Annu. Rev. Nucl. Part. Sci. **59**, 367 (2009).
[44] Q. H. Cao and C. P. Yuan, Phys. Rev. Lett. **93**, 042001 (2004).
[45] G. Balossini *et al.*, J. High Energy Phys. 01 (2010) 013.
[46] G. Corcella, I. G. Knowles, G. Marchesisni, S. Moretti, K. Odagiri, P. Richardson, M. H. Seymour, and B. R. Webber, J. High Energy Phys. 01 (2001) 010.
[47] T. Sjostrand, S. Mrenna, and P. Z. Skands, J. High Energy Phys. 05 (2006) 026.
[48] P. Richardson, R. R. Sadykov, A. A. Sapronov, M. H. Seymour, and P. Z. Skands, arXiv:1011.5444.
[49] P. Nason, J. High Energy Phys. 11 (2004) 040.
[50] S. Frixione, P. Nason, and C. Oleari, J. High Energy Phys. 11 (2007) 070.
[51] S. Alioli, P. Nason, C. Oleari, and E. Re, J. High Energy Phys. 06 (2010) 043.
[52] http://powhegbox.mib.infn.it/
[53] B. W. Harris and J. F. Owens, Phys. Rev. D **65**, 094032 (2002).
[54] H. -L. Lai *et al.*, Phys. Rev. D **82**, 074024 (2010).